

Effective strategy of enhancing piezoelectricity in stable $CrSiN_4Sn$ semiconductor monolayers by atom-layer-pair effect

Qi-Wen He(贺绮雯), Dan-Yang Zhu(朱丹阳), Jun-Hui Wang(王俊辉), He-Na Zhang(张贺娜), Xiao Shang(尚骁), Shou-Xin Cui(崔守鑫), and Xiao-Chun Wang(王晓春)

Citation: Chin. Phys. B, 2025, 34 (**5**): 057701. DOI: 10.1088/1674-1056/adb7d1
http://cpb.iphy.ac.cn; http://iopscience.iop.org/cpb

What follows is a list of articles you may be interested in

Observing ferroelastic switching in $Hf_{0.5}Zr_{0.5}O_2$ thin film

Zhao Guan(关赵), Tao Wang(王陶), Yunzhe Zheng(郑赟喆), Yue Peng(彭悦), Luqi Wei(魏鹿奇), Yuke Zhang(张宇科), Abliz Mattursun(阿卜力孜 cdot 麦提图尔荪), Jiahao Huang(黄家豪), Wen-Yi Tong(童文旖), Genquan Han(韩根全), Binbin Chen(陈斌斌), Ping-Hua Xiang(向平华), Chun-Gang Duan(段纯刚), and Ni Zhong(钟妮)
Chin. Phys. B, 2024, 33 (**6**): 067701. DOI: 10.1088/1674-1056/ad362f

Multiferroic monolayers VO*X* (*X* = Cl, Br, I): Tunable ferromagnetism via charge doping and ferroelastic switching

Hong-Chao Yang(杨洪超), Peng-Cheng Liu(刘鹏程), Liu-Yu Mu(穆鎏羽), Ying-De Li(李英德), Kai Han(韩锴), and Xiao-Le Qiu(邱潇乐)
Chin. Phys. B, 2023, 32 (**6**): 067701. DOI: 10.1088/1674-1056/acaa2b

Strain-modulated ultrafast magneto-optic dynamics of graphene nanoflakes decorated with transition-metal atoms

Yiming Zhang(张一鸣), Jing Liu(刘景), Chun Li(李春), Wei Jin(金蔚), Georgios Lefkidis, and Wolfgang Hübner
Chin. Phys. B, 2021, 30 (**9**): 097702. DOI: 10.1088/1674-1056/abeef1

First-principles calculation of influences of La-doping on electronic structures of KNN lead-free ceramics

Ting Wang(王挺), Yan-Chen Fan(樊晏辰), Jie Xing(邢洁), Ze Xu(徐泽), Geng Li(李庚), Ke Wang(王轲), Jia-Gang Wu(吴家刚), Jian-Guo Zhu(朱建国)
Chin. Phys. B, 2020, 29 (**6**): 067702. DOI: 10.1088/1674-1056/ab84db

First-principles study of polarization and piezoelectricity behavior in tetragonal $PbTiO_3$-based superlattices

Zhenye Zhu(朱振业)
Chin. Phys. B, 2018, 27 (**2**): 027701. DOI: 10.1088/1674-1056/27/2/027701

Effective strategy of enhancing piezoelectricity in stable $CrSiN_4Sn$ semiconductor monolayers by atom-layer-pair effect

Qi-Wen He(贺绮雯)[1,2], Dan-Yang Zhu(朱丹阳)[2], Jun-Hui Wang(王俊辉)[1], He-Na Zhang(张贺娜)[2], Xiao Shang(尚骁)[2], Shou-Xin Cui(崔守鑫)[1], and Xiao-Chun Wang(王晓春)[1,2,†]

[1] *School of Physics Science and Information Technology, Liaocheng University, Liaocheng* 252000, *China*
[2] *Institute of Atomic and Molecular Physics, Jilin University, Changchun* 130012, *China*

(Received 4 December 2024; revised manuscript received 7 February 2025; accepted manuscript online 19 February 2025)

It is challenging to reveal the design strategy for strong piezoelectricity nano-materials used in self-powered and smart nano-devices. Through first-principles calculations, an atom-layer-pair effect is found in $MoSi_xN_yR_z$ monolayers with remarkable piezoelectricity. The absolute values of the vertical piezoelectric coefficients have a linear relation with the total electronegativity difference dipole moments. Based on this effect, a promising $CrSiN_4Sn$ monolayer is found with the highest piezoelectricity among the above monolayers. The work expands our understanding of the piezoelectric physical mechanism and provides the design strategy for piezoelectric nano-devices.

Keywords: piezoelectricity, first-principles calculation, two-dimensional (2D) material

PACS: 77.65.–j, 71.15.–m, 73.22.–f

DOI: 10.1088/1674-1056/adb7d1 **CSTR:** 32038.14.CPB.adb7d1

1. Introduction

There has been a growing demand for miniaturized and diversified functional devices in the last few decades. Owing to their ultra-thin atomic-layer thickness,[1] piezoelectricity[2–14] and many attractive physical phenomena,[15–24] two-dimensional (2D) piezoelectric materials have great potential in nanoscale electronic device applications, such as energy harvesting, sensors and smart materials.[25–28] Vertical piezoelectricity is defined as a polarization phenomenon with polarized charge distribution in the z direction when the stress or strain is in the x, y or z direction, usually characterized by the piezoelectric stress or strain coefficients (e_{31}, e_{32}, e_{33}, d_{31}, d_{32}, or d_{33}). Vertical piezoelectricity can convert vertical mechanical energy into electricity, providing another method of energy harvesting in energy management systems.

The synthesis of $MoSi_2N_4$ monolayers,[29] as well as the MA_2Z_4 family (M = W, V, Nb, Ta, Ti, Zr, Hf, Cr; A = Si or Ge; Z = N, P, As), has been extensively explored, but they do not have vertical piezoelectricity.[30–36] Recently, the $MSi_2P_xAs_y$ and $MSiGeN_4$ have been found to exhibit weak vertical piezoelectricity ($e_{31} = -0.087 \sim 0.074 \times 10^{-10}$ C/m) due to the absence of vertical symmetry.[37–39] Vertical piezoelectricity has widespread applications in many fields, such as loudspeakers,[40] pressure sensors for bionic skin,[41] artificial intelligence materials[42] and medical implantation.[43] The reason is that these structures can vibrate up and down, making the vertical piezoelectric polarization compatible with the bottom/top gate technologies. Some reports mentioned the relation of piezoelectricity with electronegativity difference and vertical dipole moment.[4,44] However, no attention was paid to the space distribution of the atoms with different electronegative values. It is then a challenge to reveal the piezoelectric mechanism for designing high-performance materials with vertical piezoelectricity.

In this work, 39 types of Janus $MoSi_xN_yR_z$ (R = B, Al, Ga, C, Si, Ge, Sn, N, P, As, Sb, O, S, Se, Te, F or Cl; $x = 1$ or 2; $y = 2$, 3 or 4 and $z = 1$ or 2) monolayers are designed and explored, based on the architecture of a $MoSi_2N_4$ monolayer in the MA_2Z_4 family. The energy band structures, stability and Bader charge analysis calculations are performed by first-principles calculations. In response to these above challenges, we define the concept of the total electronegativity difference dipole moments to describe the space distribution of atoms with different electronegative values. An exciting piezoelectric mechanism is discovered in the four monolayers, which is further used to find a promising $CrSiN_4Sn$ monolayer with high-performance piezoelectricity. The discovery of the physical mechanism of these monolayers with vertical remarkable piezoelectricity may be valuable and expand our understanding of 2D piezoelectric materials.

2. Results and discussion

2.1. Optimal structure, electronic and stable properties of $MoSi_xN_yR_z$ monolayers

A total of 39 types of $MoSi_xN_yR_z$ (R = B, Al, Ga, C, Si, Ge, Sn, N, P, As, Sb, O, S, Se, Te, F or Cl; $x = 1$ or 2; $y = 2$, 3 or 4 and $z = 1$ or 2) monolayers are calculated in

†Corresponding author. E-mail: wangxiaochun@tsinghua.org.cn

© 2025 Chinese Physical Society and IOP Publishing Ltd. All rights, including for text and data mining, AI training, and similar technologies, are reserved.

Figs. S1–S12, with the stacking order of N/*R*–Si/*R*–N/*R*–Mo–N–Si–N. $MoSi_xN_yR_z$ monolayers possess a similar top view in Fig. 1(a). To realize the asymmetric electronic charge distribution in the monolayer along the *z* direction, only N (or Si) atom layers in the upper part of $MoSi_2N_4$ monolayer are replaced by *R* elements from the same main group as the N (or Si) element in the periodic table (Fig. 1(b)), but with different electronegativity, to obtain $MoSi_xN_yR_z$ monolayers, which may allow $MoSi_xN_yR_z$ monolayers to maintain similar electronic and atomic structures with $MoSi_2N_4$.

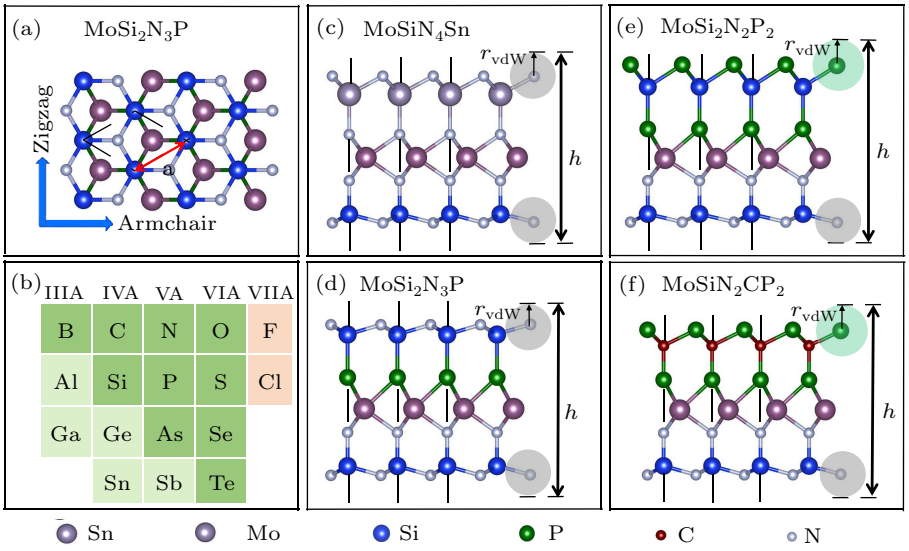


Fig. 1. (a) Top view of $MoSi_2N_3P$. (b) Periodic table displaying the atomic candidates to replace the atoms in $MoSi_2N_4$. Side views of (c) $MoSiN_4Sn$, (d) $MoSi_2N_3P$, (e) $MoSi_2N_2P_2$ and (f) $MoSiN_2CP_2$. The thickness (*h*) includes atomic Van der Waals radiuses (r_{vdW}).

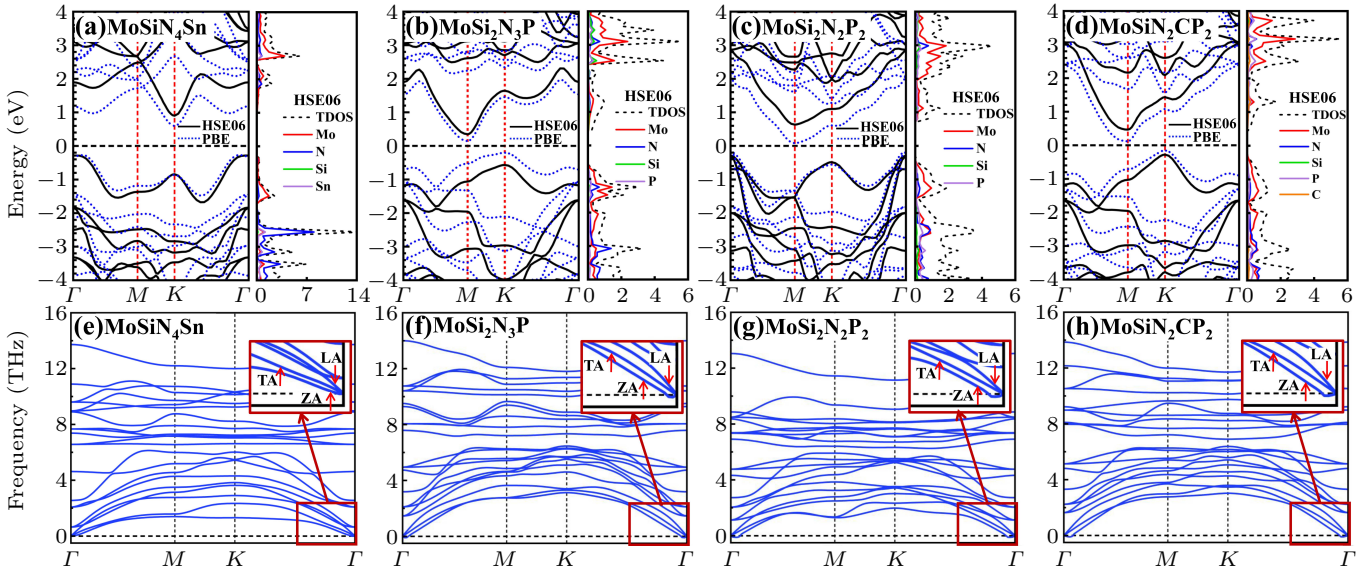


Fig. 2. (a)–(d) The band structures, PDOS with HSE06 method; and (e)–(h) phonon dispersion of $MoSiN_4Sn$, $MoSi_2N_3P$, $MoSi_2N_2P_2$ and $MoSiN_2CP_2$ monolayers, respectively. The Fermi level is set to 0 eV.

To better analyze the physical mechanism, the scopes of *R* elements are extended to the main group elements adjacent to N (or Si) element. The four stable semiconductor monolayers in Figs. 1(c)–1(f), $MoSiN_4Sn$, $MoSi_2N_3P$, $MoSi_2N_2P_2$ and $MoSiN_2CP_2$ are screened out via phonon dispersion and band structure calculations. The stacking order of $MoSiN_4Sn$ is N–Sn–N–Mo–N–Si–N, which are named as the 1st, 2nd, 3rd, 4th, 5th, 6th, and 7th atom layers, respectively. The 1st and 7th atom layers are defined as the 1st atom-layer pair. Similarly, the 2nd and 6th atom layers (and the 3rd and 5th atom layers) are the 2nd (and 3rd) atom-layer pair, respectively. Figure 1(a) shows the top view of $MoSi_2N_3P$ as a representative example of the $MoSi_xN_yR_z$ monolayers. The top view of $MoSi_2N_3P$ exhibits a hexagonal lattice, which is a common structural feature shared by all $MoSi_xN_yR_z$ monolayers. Here, each monolayer possesses three atom-layer pairs, with optimized lattice constant *a* and thickness *h* summarized in Table S1. The lattice constant and atomic thickness of $MoSi_2N_4$ are calculated to be 2.91 Å and 10.21 Å, respectively, which are consistent with Ref. [32]. The band structures and the projected density of

states (PDOS) in Figs. 2(a)–2(d) indicate the indirect bandgaps semiconductor property. An obvious peak of the N atom is observed at −2.56 eV in Fig. 2(a), indicating that many electrons are accumulated near N atoms, which mainly contribute to the negative charge of the N atoms. In Figs. S13(b)–S13(d), there is one high peak in the $-16 \sim -17$ eV range for the N atoms, rendering it negatively charged.

Similar to the research methods used in most computational references,[45–48] we calculate the phonon dispersion, *ab initio* molecular dynamics (AIMD) and formation energy to clarify the stability and synthesis possibility of these materials. The phonon dispersions are shown in Figs. 2(e)–2(h). There are three acoustic branches converged at the high symmetric Γ point. The out-of-plane branch ZA with the lowest frequency among the acoustic branches is in a parabolic relationship with the wave vector near the Γ point, while the transverse in-plane branch TA and the longitudinal in-plane branch LA have linear dispersion near the Γ point.[49,50] All four monolayers exhibit no imaginary frequencies near the Γ point, demonstrating that they are dynamically stable. Meanwhile, AIMD simulations with the 112 atoms in a $4\times4\times1$ supercell are carried out. After running for more than 3000 fs with a time step of 1 fs at 300 K, the data (Fig. S14) proves the thermodynamic stability of these monolayers. Furthermore, all the formation energies (E_f) of these monolayers ($E_f = -1.96 \sim -3.79$ eV) are negative in Table S1. It is likely that these monolayers can be synthesized experimentally, just as the $MoSi_2N_4$ monolayer with a similar structure to these monolayers has been experimentally synthesized.[29]

2.2. Elastic and piezoelectric properties of the $MoSi_xN_yR_z$ monolayer

The elastic properties indicate that all four monolayers are mechanically stable, meeting the Born–Huang criteria:[10,51] $C_{11}C_{22} - C_{12}^2 > 0$ and $C_{66} > 0$ (Table S2). The Young's moduli (311.65 ∼ 418.00 N/m) of these monolayers with isotropic elasticity (Fig. S15) are larger than that of MoS_2 (130 N/m),[52] and some are even greater than that for graphene (340 N/m).[53,54] This suggests the four monolayers can withstand greater strain, thus possessing potential applications in special environments.

The in-plane piezoelectric coefficients (e_{22} and d_{22}) and vertical piezoelectric coefficients (e_{31}, e_{33}, d_{31} and d_{33}) of the four monolayers are summarized in Table 1. $MoSiN_2CP_2$ possesses the largest e_{31} with 1.37×10^{-10} C/m among the four monolayers due to broken inversion symmetry, outperforming $MSi_2P_xAs_y$ ($e_{31} = 0.011 \sim 0.074\times10^{-10}$ C/m)[37] and SnS ($e_{31} = 0.30\times10^{-10}$ C/m).[39,55,56] The piezoelectric coefficient of e_{33} reflects the vertical piezoelectricity of the monolayer under vertical strain, which is more practical than e_{22} and e_{31}. The e_{33} values of the four monolayers are between -0.34×10^{-10} and 1.16×10^{-10} C/m, comparable to Zr_2P_2ICl ($e_{33} = 0.61\times10^{-10}$ C/m)[57] and Te_2Se multilayers ($0.37 \sim 1.52\times10^{-10}$ C/m).[58] Furthermore, among the four monolayers, $MoSi_2N_2P_2$ exhibits the best in-plane piezoelectric properties with $|e_{22}| = 9.22\times10^{-10}$ C/m, which is $2.5 \sim 48.5$ times larger than that of the known MA_2Z_4 family ($0.19 \sim 3.69\times10^{-10}$ C/m).[32] The results prove that the replacement of partial atoms in $MoSi_2N_4$ can increase both vertical and in-plane piezoelectricity. Additionally, Born effective charges $Z^*_{k,ij}$ related to the ionic contribution are further summarized in Table S3. According to Table S4, the negative e_{33} of $MoSiN_4Sn$ is attributed to the negative ionic contribution over the positive electronic contribution, while the positive e_{33} of $MoSi_2N_2P_2$ and $MoSiN_2CP_2$ are dominated by a large electronic contribution. The relaxed-ion piezoelectric coefficients are composed of electronic and ionic contributions. Therefore, the Born effective charge $Z^*_{k,ij}$ cannot directly determine the piezoelectric coefficients e_{33}.

Table 1. The relaxed-ion piezoelectric coefficients of $MoSiN_4Sn$, $MoSi_2N_3P$, $MoSi_2N_2P_2$ and $MoSiN_2CP_2$. The units of e and d are 10^{-10} C/m and pm/V, respectively.

Material	e_{22}	e_{31}	e_{33}	d_{22}	d_{31}	d_{33}
$MoSiN_4Sn$	−5.75	−0.26	−0.34	−2.16	−0.03	−0.24
$MoSi_2N_3P$	−6.92	0.84	0.16	−2.04	0.14	0.12
$MoSi_2N_2P_2$	−9.22	1.24	1.16	−3.57	0.12	−0.42
$MoSiN_2CP_2$	−4.63	1.37	0.66	−1.37	0.16	−0.78

The static polarization charge distribution is further discussed by Bader charge analysis (Fig. S16). In $MoSi_xN_yR_z$ monolayers, N atoms with the largest electronegativity gain the most electrons, followed by C atoms. Here, $MoSi_xN_yR_z$ monolayers are divided into upper (including the 1st, 2nd and 3rd atom layers) and lower (including the 5th, 6th and 7th atom layers) parts by the middle Mo atom layer. The difference in electronegativity of atoms in the atom-layer pair contributes to an uneven vertical distribution of electrons, giving rise to a local dipole moment in $MoSi_xN_yR_z$ monolayers. Such as $MoSiN_4Sn$, for the 2nd atom-layer pair, the electronegativity 1.96 of Sn atom in the 2nd atom layer is larger than that 1.90 of Si in the 6th atom layer. The atom electronegativity is the same for atoms in the 1st (or 3rd) atom-layer pair. Then, the electron transformed from the Mo atom to the upper part (N-SnN region) with a net charge of $-0.767|e|$ is a little higher than that to the lower part (N–Si–N region) with a net charge of $-0.754|e|$. The 2D charge density difference (Fig. S17) indicates that, except for the Mo atom forming a partial covalent bond with P atom in $MoSiN_2CP_2$ (Fig. S17(d)), the other atoms in the four monolayers form ionic bonds.

We define the concept of the total electronegativity difference dipole moments (TED-dipole moments) P_{TED}. The P_{TED} for $MoSi_xN_yR_z$ monolayers can be given by

$$P_{TED} = \sum_{i=1}^{3} \left[\left(ELN_L^i - ELN_{Mo} \right) \times h_{L^i-Mo} \right.$$

$$+\left(\mathrm{ELN_{Mo}}-\mathrm{ELN_U^i}\right)\times h_{\mathrm{Mo-U^i}}\Big], \quad (1)$$

where i is the ordinal of atom-layer pair; L (U) is the lower (upper) atom layer, $\mathrm{ELN_L^i}(\mathrm{ELN_U^i})$ denotes the electronegativity of the lower (upper) atom layer in the ith atom-layer pair and $\mathrm{ELN_{Mo}}$ represents the electronegativity of the Mo atom in the middle atom layer. $h_{\mathrm{L}^i-\mathrm{Mo}}(h_{\mathrm{Mo-U}^i})$ means the vertical distance between L^i (U^i) atom and the middle atom (see Table S1). $\left(\mathrm{ELN_L^i}-\mathrm{ELN_{Mo}}\right)\times h_{\mathrm{L}^i-\mathrm{Mo}}$ ($\left(\mathrm{ELN_{Mo}}-\mathrm{ELN_U^i}\right)\times h_{\mathrm{Mo-U}^i}$) represents the electronegativity difference dipole moments (ED-dipole moments) between the lower (and upper) ith atom layer and the Mo atom layer. The microscopic mechanism of Eq. (1) is that TED-dipole moments approximately describe the contributions of each atom-layer pair to the asymmetric vertical polarization in the monolayer, which also includes the contribution of the polarization charge direction in each atom-layer pair. The larger TED-dipole moments suggest a larger degree of asymmetric vertical polarization in the monolayer, which may result in larger vertical piezoelectricity.

In a certain atom-layer pair, when $\left(\mathrm{ELN_L^i}-\mathrm{ELN_{Mo}}\right)$ and $\left(\mathrm{ELN_{Mo}}-\mathrm{ELN_U^i}\right)$ are both positive (or negative), the total polarization charge of the 2D structure will be enhanced. This phenomenon is defined as the positive-cascade effect, resulting in the TED-dipole moments increase. However, when the $\left(\mathrm{ELN_L^i}-\mathrm{ELN_{Mo}}\right)$ is positive (or negative), but the $\left(\mathrm{ELN_{Mo}}-\mathrm{ELN_U^i}\right)$ is negative (or positive), the total polarization charge of the 2D structure will be weakened. This phenomenon is defined as the negative-cascade effect, leading to the TED-dipole moments decrease. The positive/negative-cascade effect effectively reveals the physical significance of the TED-dipole moments. Equation (1) can describe both of the above situations well. Figure 3(a) shows the mechanism of the positive/negative-cascade effect, using the 3rd atom-layer pair of the $\mathrm{MoSi}_x\mathrm{N}_y R_z$ monolayers as an example. Specifically, in the $\mathrm{MoSi_2N_2P_2}$ monolayer, both $\left(\mathrm{ELN_N^3}-\mathrm{ELN_{Mo}}\right)$ and $\left(\mathrm{ELN_{Mo}}-\mathrm{ELN_P^3}\right)$ are negative, resulting in a positive-cascade effect for the total polarization charge. In contrast, for the $\mathrm{MoSiN_2CP_2}$ monolayer, the $\left(\mathrm{ELN_{Si}^2}-\mathrm{ELN_{Mo}}\right)$ is negative, while the $\left(\mathrm{ELN_{Mo}}-\mathrm{ELN_C^2}\right)$ is positive, leading to a negative-cascade effect of the total polarization charge.

The piezoelectric performance can be evaluated by the absolute value of piezoelectric coefficients. The black data line in Fig. 3(b) shows that for $\mathrm{MoSi}_x\mathrm{N}_y R_z$ monolayers, the larger absolute values of TED-dipole moments ($|P_{\mathrm{TED}}|$) lead to larger vertical polarization and larger $|e_{33}|$, and the relationship P_{TED} is almost a linear function. This fact is defined as the atom-layer pair effect by us. Notably, the P_{TED} of $\mathrm{MoSi_2N_4}$ ($e_{33}=0$ C/m) equals zero due to its mirror symmetry along the z direction and this point is called the zero point of the black data line in Fig. 3(b). Due to the $\mathrm{MoSi_2N_2P_2}$ with smaller electronegativity 2.19 of the 1st atom layer (P atom) than that 3.04 of the 1st atom layer (N atom) in the $\mathrm{MoSi_2N_3P}$, the $\left(\mathrm{ELN_{Mo}}-\mathrm{ELN_P^1}\right)=-0.03$ of $\mathrm{MoSi_2N_2P_2}$ is larger than $\left(\mathrm{ELN_{Mo}}-\mathrm{ELN_N^1}\right)=-0.88$ of $\mathrm{MoSi_2N_3P}$. The $\left(\mathrm{ELN_{Mo}}-\mathrm{ELN_P^1}\right)\times h_{\mathrm{Mo-P^1}}=-0.15$ Å of $\mathrm{MoSi_2N_2P_2}$ is larger than $\left(\mathrm{ELN_{Mo}}-\mathrm{ELN_N^1}\right)\times h_{\mathrm{Mo-N^1}}=-3.84$ Å of $\mathrm{MoSi_2N_3P}$, although $h_{\mathrm{Mo-P^1}}$ (4.95 Å) $>h_{\mathrm{Mo-N^1}}$ (4.36 Å). It leads to the greater deviation of $P_{\mathrm{TED}}^{\mathrm{MoSi_2N_2P_2}}$ from the zero point than that of $P_{\mathrm{TED}}^{\mathrm{MoSi_2N_3P}}$. According to the atom-layer pair effect, the $|e_{33}|$ of $\mathrm{MoSi_2N_2P_2}$ may be larger than that of $\mathrm{MoSi_2N_3P}$. The calculated e_{33} values in Table 1 prove the above analytic results. Notably, the atom-layer-pair effect takes into account the space distribution of atoms with different electronegative values well, which is a good supplement to previous research without considering the space distribution.[4,44]

Based on the atom-layer-pair effect, we predict high-performance piezoelectric material. We replace the Mo atom in the above four stable semiconductors with a Cr atom to get three stable monolayers, $\mathrm{CrSiN_4Sn}$, $\mathrm{CrSi_2N_3P}$ and $\mathrm{CrSiN_2CP_2}$, with large vertical piezoelectricity (Figs. S18–S20). Especially, the $\mathrm{CrSiN_4Sn}$ monolayer has the largest e_{33} ($e_{33}=11.93\times10^{-10}$ C/m) among all the seven monolayers calculated in this work. It is larger than the $e_{31}=1.20\times10^{-10}$ C/m of $\mathrm{La_2CO_2}$[10] by 9.94 times and the $e_{13}=1.40\times10^{-10}$ C/m of MoSO[59] by 8.52 times.

Notably, the data points about the $|e_{33}|$ and the $|P_{\mathrm{TED}}|$ of $\mathrm{CrSiN_4Sn}$ and $\mathrm{CrSi_2N_3P}$ monolayers are on the same blue data line in Fig. 3(b), while that of the $\mathrm{CrSiN_2CP_2}$ is not on this blue data line. To explain this, we propose the "window effect" of electronegativity difference based on the data in this work.

There are some predefinitions for this window effect. (i) We define the zero-point structures, which are the structures with data points at the zero point (0, 0) in Fig. 3(b). For example, $\mathrm{MoSi_2N_4}$ and $\mathrm{CrSi_2N_4}$ with $e_{33}=0$ C/m are the zero-point-structures. (ii) In Fig. 3(b), the structures corresponding to the data points on the same data line with a certain slope are named as the structure group.

These are the contents of the window effect: (i) The window effect is only used to discuss the atoms in the other structure that are different from the atoms in the zero-point structure and ignores the same atoms relative to the zero-point structure. (ii) For each structure in the certain structure group, the electronegativity difference between the atoms using the window effect and the atom of the middle atom layer should be within a certain value range. This range is named the electronegativity-difference window. If the electronegativity difference is not within the electronegativity-difference window, the data points in Fig. 3(b) will not be on the data line corresponding to the same structure group.

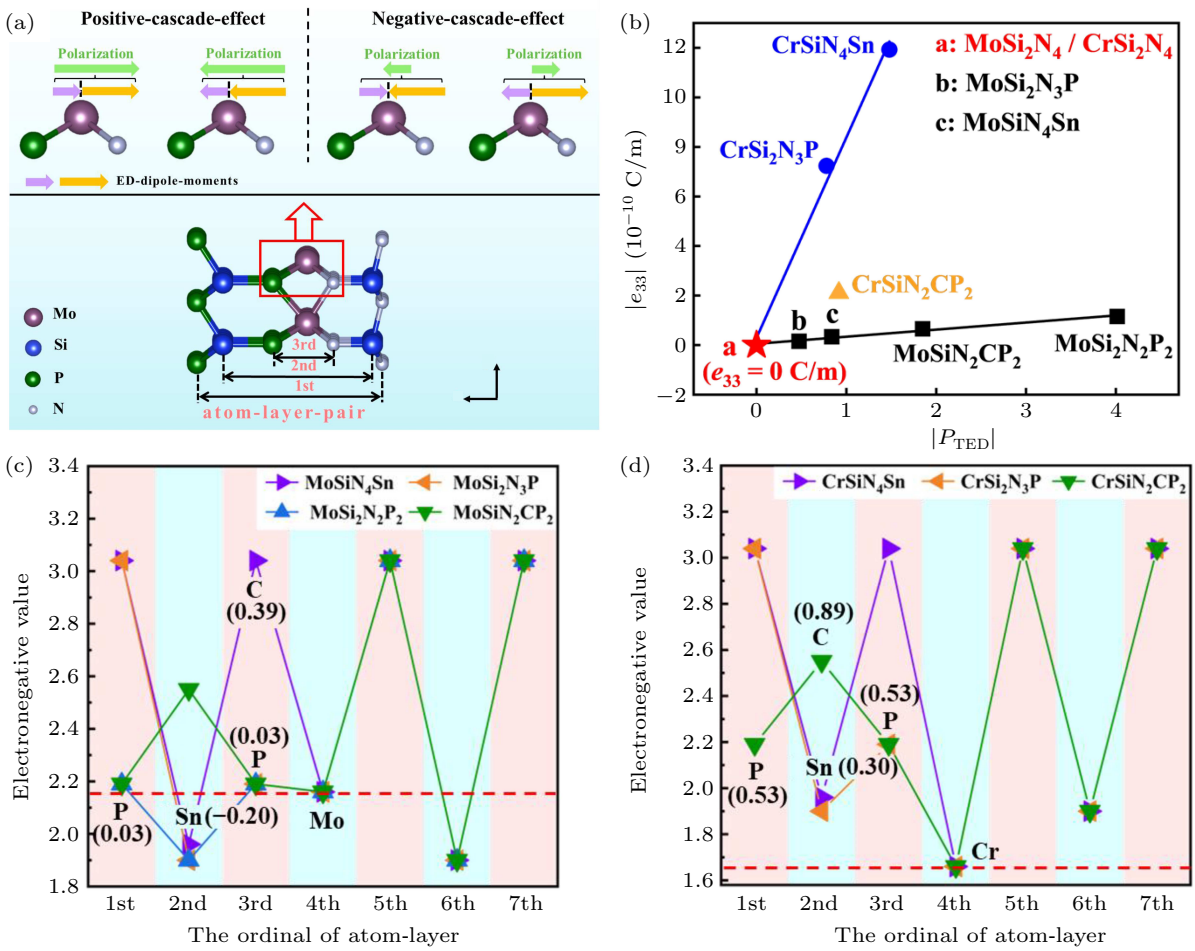


Fig. 3. (a) The positive/negative-cascade effect in the $MoSi_xN_yR_z$ monolayers. (b) The relationship between the absolute value of e_{33} ($|e_{33}|$) and the absolute value of TED-dipole moments ($|P_{TED}|$). The electronegative values in the (c) $MoSi_xN_yR_z$ and (d) $CrSi_xN_yR_z$ monolayers, respectively. The values in parentheses stand for the electronegativity differences of the atoms relative to the (c) Mo atom and (d) Cr atom, respectively.

Figures 3(c) and 3(d) show the electronegativity difference between the atoms using the window effect and the m atom. Each monolayer has the same atoms in the 5th $\sim$ 7th atom layers. For the four $MoSi_xN_yR_z$ monolayers, the relatively small range of the electronegativity difference ($-0.20 \sim 0.39$) in Fig. 3(c) is within the electronegativity-difference window. Therefore, these monolayers are regarded as the same structure group, corresponding to the black data line in Fig. 3(b). Additionally, in Fig. 3(c), the range of 0.3 to 0.53 in the electronegativity difference is relatively small and within the electronegativity-difference window. Hence, $CrSiN_4Sn$ and $CrSi_2N_3P$ monolayers are viewed as a structure group corresponding to the blue data line. For these monolayers, the $CrSi_2N_3P$ monolayer with the electronegativity difference of 0.53 is on the blue data line in Fig. 3(b), while the data of $CrSiN_2CP_2$ with the electronegativity difference of 0.89 between C atom and Cr atom is not on the blue data line of the same structure group. Therefore, we speculate that there is an upper limit of the electronegativity-difference window in the range of 0.53 to 0.89, and the data of monolayers within the upper limit are on the same blue data line. Strikingly, both the blue and black data lines of different structure groups cross the same zero point, which is a very special property. Here, we name the blue and black data lines as atom-layer-pair-effect data lines. Furthermore, different atoms in the middle atom layer with different electronegativity can directly affect the P_{TED} according Eq. (1). Therefore, the monolayers in the same structure group have the same atom in the middle atom layer. Overall, the atom-layer-pair effect can reveal the vertical piezoelectric physical mechanism of these seven monolayers in this work combined with the window effect of electronegativity difference, deepening the physical understanding of piezoelectric properties.

Equation (1) can also be extended to the odd multi-atom-layer 2D semiconductors with similar asymmetric structures. There are n atom-layer pairs ($n = 1, 2, 3, \ldots$) in the odd multi-atom-layer with one atom layer as the middle atom layer, which is named the Z monolayer. The L^j and U^j atom layers are viewed as an atom-layer pair, where the j is the ordinal of the atom-layer pair. ELN_L^j (ELN_U^j) stands for the electronegativity of the lower (upper) atom in the ith atom-layer pair. Then the TED-dipole moment of odd multi-atom-layer mono-

layer may be derived as

$$P_{\mathrm{TED}} = \sum_{j=1}^{n} \left[\left(\mathrm{ELN}_{\mathrm{L}}^{j} - \mathrm{ELN}_{m} \right) \times h_{\mathrm{L}^{j}-m} + \left(\mathrm{ELN}_{m} - \mathrm{ELN}_{\mathrm{U}}^{j} \right) \times h_{m-\mathrm{U}^{j}} \right]. \quad (2)$$

The extended atom-layer-pair effect (based on Eq. (2)) has been proved with reasonable results when $j = 3$ for $MoSi_xN_yR_z$ monolayers in this work.

3. Conclusion

In summary, $MoSiN_4Sn$, $MoSi_2N_3P$, $MoSi_2N_2P_2$ and $MoSiN_2CP_2$ monolayers, as hopeful piezoelectric materials, are predicted and fully discussed by first-principles calculations. Interestingly, the piezoelectric coefficient $|e_{33}|$ shows a good linear relation with the $|P_{\mathrm{TED}}|$ that is defined as the TED-dipole moments P_{TED}. This phenomenon is named the atom-layer-pair effect. The atom-layer-pair effect takes into account the space distribution of atoms with different electronegative values and also considers the positive/negative-cascade effect. Significantly, this effect is further used to find the $CrSiN_4Sn$ monolayer with remarkably strong vertical piezoelectric properties, superior to another studied MA_2Z_4 family by at least 20 times. These 2D materials with high piezoelectricity can be promising candidates for the fundamental units to effectively generate practical voltage outputs by appropriately stacking them into multilayered structures. Moreover, two concepts of the zero-point structure and the window effect of electronegativity difference are proposed to make the atom-layer-pair effect more applicable. We hope that this work can provide an approach to understanding the intrinsic physical mechanisms of high-performance 2D piezoelectric materials with similar structures.

Acknowledgment

Project supported by the National Natural Science Foundation of China (Grant No. 11474123).

References

[1] Qiao H, Wang C, Choi W S, Park M H and Kim Y 2021 *Mat. Sci. Eng. R* **145** 100622
[2] Jia H J, Mu H M, Li J P, Zhao Y Z, Wu Y X and Wang X C 2018 *Phys. Chem. Chem. Phys.* **20** 26288
[3] Wu Y, Yang C H, Zhang H N, Zhu L H, Wang X Y, Li Y Q, Zhu S Y and Wang X C 2022 *Appl. Surf. Sci.* **589** 152999
[4] Zhang H N, Wu Y, Yang C, Zhu L H and Wang X C 2021 *Phys. Rev. B* **104** 235437
[5] Zhang H N, Yang C, Li Y Q, Zhu S Y, Wang X Y, He Q W, Tang D S and Wang X C 2022 *Appl. Phys. Lett.* **121** 143504
[6] Li Y Q, Wang X Y, Zhu S Y, Tang D S, He Q W and Wang X C 2022 *J. Mater. Chem. C* **10** 12132
[7] Li Y Q, Wang X Y, Zhu S Y, Tang D S, He Q W and Wang X C 2022 *J. Phys. Chem. Lett.* **13** 9654
[8] Zhu D R, Wu Y, Zhang H N, Zhu L H, Zhao S N and Wang X C 2020 *Physica E* **124** 114214
[9] Zhao Y Z, Jia H J, Zhao S N, Wang Y B, Li H Y, Zhao Z L, Wu Y X and Wang X C 2020 *Physica E* **117** 113817
[10] Tan J, Wang Y, Wang Z, He X, Liu Y, Wang B, Katsnelson M I and Yuan S 2019 *Nano Energy* **65** 104058
[11] Li F, Shen T, Wang C, Zhang Y, Qi J and Zhang H 2020 *Nano-Micro Letters* **12** 106
[12] He Q W, Zhu D Y, Tang D S, Shang X, Wang J H, Zhang G Q, Liu F and Wang X C 2024 *Chin. J. Phys.* **91** 147
[13] Liu X, Wang R, Wang X, Zhang W, Dong Y, Du R R, Liu Y and Lin X 2024 *Chin. Phys. Lett.* **41** 047301
[14] Jin C F, Zhang S Q, Shen Z Q and Li W L 2019 *Chin. Phys. Lett.* **36** 107701
[15] Li J P, Jia H J, Zhu D R, Wang X C, Liu F C and Yang Y J 2019 *Appl. Surf. Sci.* **463** 918
[16] Wu Y, Yu H X, Yang C H, Zhang H N, Zhu L H, Ma Y, Wang X C and Zhang S 2021 *Int. J. Hydrogen Energ.* **46** 34216
[17] Liu L L, Wang Y, Chen C P, Yu H X, Zhao L S and Wang X C 2017 *RSC Advances* **7** 40200
[18] Wang X Y, Li Y Q, Zhu S Y, Tang D S, He Q W and Wang X C 2022 *J. Membrane Sci.* **662** 121030
[19] Gao W and Chelikowsky J R 2020 *Nano Lett.* **20** 8346
[20] Ma N G, Zhang Y J, Zhang H N, Mu H M, Zhang Y and Wang X C 2023 *Appl. Surf. Sci.* **628** 157315
[21] Li Y Q, Tang D S, He Q W, Shang X and Wang X C 2023 *Appl. Phys. Lett.* **122** 193903
[22] He Q W, Wu Y, Yang C H, Zhang H N, Tang D S, Shang X and Wang X C 2023 *Nanoscale* **15** 10458
[23] Cheng Y C, Zhu Z Y, Tahir M and Schwingenschlögl U 2013 *Europhys. Lett.* **102** 57001
[24] He Q W, Wang J H, Zhu D Y, Tang D S, Lv Z, Guo F and Wang X C 2024 *Nano Lett.* **24** 8979
[25] Liu L, Guo X and Lee C 2021 *Nano Energy* **88** 106304
[26] Mahmud M A P, Bazaz S R, Dabiri S, Mehrizi A A, Asadnia M, Warkiani M E and Wang Z L 2022 *Adv. Mater. Technol.* **7** 2101347
[27] Zhou H, Zhang Y, Qiu Y, Wu H, Qin W, Liao Y, Yu Q and Cheng H 2020 *Biosens. Bioelectron.* **168** 112569
[28] Nan Y, Tan D, Shao J, Willatzen M and Wang Z L 2021 *ACS Energy Letters* **6** 2313
[29] Hong Y L, Liu Z B, Wang L, Zhou T Y, Ma W, Xu C, Feng S, Chen L, Chen M L, Sun D M, Chen X Q, Cheng H M and Ren W C 2020 *Science* **369** 670
[30] Yang C, Song Z, Sun X and Lu J 2021 *Phys. Rev. B* **103** 035308
[31] Sibatov R T, Meftakhutdinov R M and Kochaev A I 2022 *Appl. Surf. Sci.* **585** 152465
[32] Mortazavi B, Javvaji B, Shojaei F, Rabczuk T, Shapeev A V and Zhuang X 2021 *Nano Energy* **82** 105716
[33] Wang Y and Ding Y 2021 *Appl. Phys. Lett.* **119** 193101
[34] Tian M, Wei C H, Zhang J L, Wang J and Yang R Z 2021 *Phys. Rev. B* **103** 195305
[35] Mohebpour M A, Mortazavi B, Rabczuk T, Zhuang X Y, Shapeev A V and Tagani M B 2022 *Phys. Rev. B* **105** 134108
[36] Yin Y, Gong Q, Yi M and Guo W 2023 *Adv. Funct. Mater.* **33** 2301234
[37] Rezavand A, Ghobadi N and Behnamghader B 2022 *Phys. Rev. B* **106** 035417
[38] Yu Y, Zhou J, Guo Z and Sun Z 2021 *ACS Appl. Mater. Interfaces* **13** 28090
[39] Guo S D, Mu W Q, Zhu Y T, Han R Y and Ren W C 2021 *J. Mater. Chem. C* **9** 2464
[40] Scheeper P R, van der Donk A G H, Olthuis W and Bergveld P 1994 *Sensor Actuat. A-Phys.* **44** 1
[41] Zheng Q, Shi B, Li Z and Wang Z L 2017 *Adv. Sci.* **4** 1700029
[42] Mahapatra S D, Mohapatra P C, Aria A I, Christie G, Mishra Y K, Hofmann S and Thakur V K 2021 *Adv. Sci.* **8** e2100864
[43] Park D Y, Joe D J, Kim D H, Park H, Han J H, Jeong C K, Park H, Park J G, Joung B and Lee K J 2017 *Adv. Mater.* **29** 1702308
[44] Kaur A, Sharma S, Nandi P and De Sarkar A 2023 *Physica E* **154** 115791
[45] Zhang S, Zhou J, Wang Q, Chen X, Kawazoe Y and Jena P 2015 *Proc. Natl. Acad. Sci. USA* **112** 2372
[46] Yafei Li Z Z, Shengbai Zhang and Zhongfang Chen 2008 *J. Am. Chem. Soc.* **130** 16739
[47] Cahangirov S, Topsakal M, Aktürk E, Şahin H and Ciraci S 2009 *Phys. Rev. Lett.* **102** 236804
[48] Wu T and Wang J 2019 *Nano Energy* **66** 104070

[49] Shen C, Wang L, Wei D, Zhang Y, Qin G, Chen X Q and Zhang H 2022 *Phys. Chem. Chem. Phys.* **24** 3086

[50] Jiang J W, Wang B S, Wang J S and Park H S 2015 *J. Phys. Condens. Matter.* **27** 083001

[51] Varjovi M J, Ershadrad S and Sanyal B 2023 *Phys. Rev. B* **107** 195421

[52] Cooper R C, Lee C, Marianetti C A, Wei X, Hone J and Kysar J W 2013 *Phys. Rev. B* **87** 035423

[53] Andrew R C, Mapasha R E, Ukpong A M and Chetty N 2012 *Phys. Rev. B* **85** 125428

[54] de Jong M, Chen W, Geerlings H, Asta M and Persson K A 2015 *Sci. Data* **2** 150053

[55] Guo Y, Zhou S, Bai Y and Zhao J 2017 *Appl. Phys. Lett.* **110** 163102

[56] Dai Y, Zhang X, Cui Y, Li M, Luo Y, Jiang F, Zhao R and Huang Y 2021 *Nano Res.* **15** 209

[57] Li Y Q, Zhang H N, Yang C, Wang X Y, Zhu S Y and Wang X C 2023 *Appl. Surf. Sci.* **608** 155202

[58] Chen Y, Liu J, Yu J, Guo Y and Sun Q 2019 *Phys. Chem. Chem. Phys.* **21** 1207

[59] Yagmurcukardes M and Peeters F M 2020 *Phys. Rev. B* **101** 155205